

Postsynthetic Metalation of a Robust Hydrogen-Bonded Organic Framework for Heterogeneous Catalysis

Bin Han,[†] Hailong Wang,^{*,†} Chiming Wang,[†] Hui Wu,[§] Wei Zhou,[§] Banglin Chen,^{*,†} and Jianzhuang Jiang^{*,†}[†]Beijing Key Laboratory for Science and Application of Functional Molecular and Crystalline Materials, Department of Chemistry, University of Science and Technology Beijing, Beijing 100083, China[‡]Department of Chemistry, University of Texas at San Antonio, San Antonio, Texas 78249-0698, United States[§]Center for Neutron Research, National Institute of Standards and Technology, Gaithersburg, Maryland 20899-6102, United States

Supporting Information

ABSTRACT: Hydrogen-bonded organic framework (HOF)-based catalysts still remain unreported thus far due to their relatively weak stability. In the present work, a robust porous HOF (HOF-19) with a Brunauer–Emmett–Teller surface area of 685 m² g^{−1} was reticulated from a cage-like building block, amino-substituted bis-(tetraoxacalix[2]arene[2]triazine), depending on the hydrogen bonding with the help of π – π interactions. The postsynthetic metalation of HOF-19 with palladium acetate afforded a palladium(II)-containing heterogeneous catalyst with porous hydrogen-bonded structure retained, which exhibits excellent catalytic performance for the Suzuki–Miyaura coupling reaction with the high isolation yields (96–98%), prominent stability, and good selectivity. More importantly, by simple recrystallization, the catalytic activity of deactivated species can be recovered from the isolation yield 46% to 92% for 4-bromobenzonitrile conversion at the same conditions, revealing the great application potentials of HOF-based catalysts.

Heterogeneous catalysis plays a dominant role in the chemical and pharmaceutical industry.¹ As a result, continuous efforts have been paid toward developing effective methods for synthesizing heterogeneous catalysts with high efficiency and in particular with an easy recovery and recycling nature. In the past several years, by immobilizing homogeneous catalysts inside the porous supports such as zeolites,² metal–organic frameworks (MOFs),³ and covalent organic frameworks (COFs),⁴ diverse heterogeneous catalysts with boosted activity and stability have been fabricated. However, the regeneration of these heterogeneous catalysts is still challenging due to their nonrenewable porous supports.

In the same way as MOFs and COFs, porous hydrogen-bonded organic frameworks (HOFs) are self-assembled from discrete molecular modules as well.⁵ Despite the outstanding properties of HOFs revealed in the fields of gas storage,⁶ small-molecule separation,⁷ sensing,⁸ and proton conduction,⁹ reports over HOF-based catalysts still remain unknown, to the best of our knowledge, due to the relatively poor stability associated with the weak hydrogen bonding connection between discrete building blocks in HOFs.^{5–9} Fortunately, the introduction of

additional π – π interactions would significantly enhance the stability when aromatic building blocks are employed for constructing HOFs,^{5g,6f} rendering it possible to fabricate heterogeneous catalysts with robust frameworks as the porous support of homogeneous species. In particular, the excellent recyclability of HOFs through simple recrystallization enables them to be regenerated easily, thus endowing the sustainable advantage to HOF-based catalysts.

Herein, a novel organic cage of amino-substituted bis-(tetraoxacalix[2]arene[2]triazine) (L) composed of five six-membered aromatic rings has been designed and prepared as a building block for assembling HOFs (Figure 1a and Scheme S1, Supporting Information). Depending on the hydrogen bonding between neighboring building blocks with the help of rich π – π interactions between intercage aromatic moieties, the first cage-

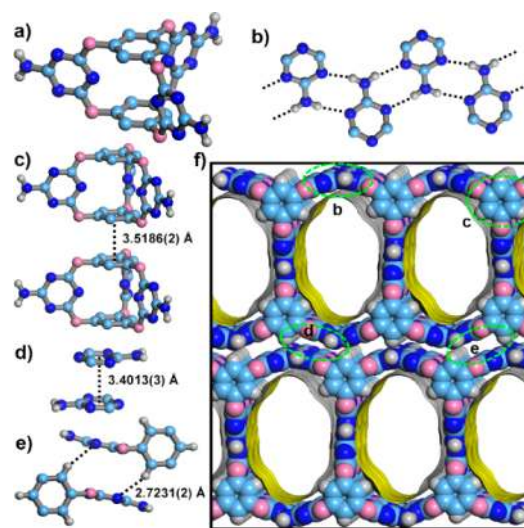


Figure 1. Crystal structure of HOF-19 showing (a) molecular organic cage L; (b) hydrogen bonding ribbon comprising neighboring AT groups; (c, d) two kinds of intercage cofacial π – π interactions; (e) the C–H... π interaction; and (f) a packing diagram of HOF-19 showing the 1D channel surfaces highlighted as yellow/gray (inner/outer) curved planes (C, slight cyan; O, pink; N, blue; H, white).

Received: April 8, 2019

Published: May 22, 2019



based HOF (HOF-19) is constructed, and its hydrogen-bonded structure is clearly revealed by single-crystal X-ray diffraction analysis. The N_2 sorption measurement at 77 K discloses a Brunauer–Emmett–Teller (BET) surface area of $685\text{ m}^2\text{ g}^{-1}$ for activated HOF-19. Postfunctionalization of this HOF with palladium acetate gives a palladium(II)-containing HOF-19 \supset Pd(II) with parent hydrogen-bonded structure maintained according to the powder X-ray diffraction (PXRD) analysis, indicating the robustness of HOF-19. Further evidence on the robustness of HOF-19 comes from the excellent stability and recyclability of HOF-19 \supset Pd(II) in *p*-xylene in the presence of potassium carbonate at $150\text{ }^\circ\text{C}$. Under such experimental conditions, the Suzuki–Miyaura coupling reaction is able to be selectively promoted in high isolation yields (96–98%), revealing the predominant catalytic activity of HOF-based materials for the first time. Nevertheless, the catalytic activity of deactivated species, with the 46% isolation yield for the conversion of 4-bromobenzonitrile, is recovered to 92% by simple recrystallization regeneration, revealing the great application potentials of HOF-based catalysts.

A facile reaction between chloride-substituted bis-(tetraoxacalix[2]arene[2]triazine)¹⁰ and ammonium hydroxide afforded **L** (Scheme S1 and Figures S1 and S2, Supporting Information). The slow evaporation of the formic acid solution of **L** gave single crystals of HOF-19 with poor solubility in common organic solvents (except only DMSO). Single-crystal X-ray diffraction data confirms the three-dimensional (3D) porous structure of HOF-19 (Figure 1; Tables S1 and S2, Supporting Information). As exhibited in Figure 1, depending on the multiple N–H \cdots N hydrogen bonding between interstage 2-aminotriazinyl (AT) groups with the help of π – π interactions from interstage benzene moieties, two-dimensional porous hydrogen-bonded supramolecular structures containing one-dimensional (1D) channels with the size of $8.0 \times 13.6\text{ \AA}$ along the [010] direction are formed, which are further packed into the 3D architecture of HOF-19 depending on the interstage cofacial π – π interaction between AT groups and C–H \cdots π interaction (actually a kind of π – π interaction). The PLATON calculation discloses 47% void space for HOF-19,¹¹ which should be favorable for the molecular substrate diffusion.

The bulk material of HOF-19 with good thermal stability was obtained by diffusing acetone into the formic acid solution of **L** (Figure S3, Supporting Information). Acetone-exchanged HOF-19 was degassed at $25\text{ }^\circ\text{C}$ to give an activated sample (HOF-19a). The PXRD pattern of HOF-19a is well consistent with the simulated profile of HOF-19 (Figures S4 and S5, Supporting Information), indicating its robust nature. The N_2 sorption measurement at 77 K reveals its type I adsorption curve with a N_2 uptake of $287\text{ cm}^3\text{ g}^{-1}$ at 1.0 bar (Figure 2). The experimental pore volume of $0.45\text{ cm}^3\text{ g}^{-1}$ is well consistent with the theoretical value ($0.48\text{ cm}^3\text{ g}^{-1}$; Table S1).¹¹ The BET surface area of HOF-19a was calculated to be $685\text{ m}^2\text{ g}^{-1}$.

The multiple hydrogen bonding and π – π interactions between neighboring cages enhance the robustness of HOF-19. The poor solubility of HOF-19 in common organic solvents could effectively stabilize the framework in solution. In addition, abundant triazinyl nitrogen atoms and amino groups inside the pores of HOF-19 provide enough binding sites to incorporate catalytically active metal ions. All these characteristics inspire us to fabricate a heterogeneous catalyst with HOF-19 as the porous support. The immersion of activated HOF in an acetone solution of palladium acetate (0.100 mM) afforded palladium(II)-containing HOF-19 \supset Pd(II). Its PXRD pattern matches

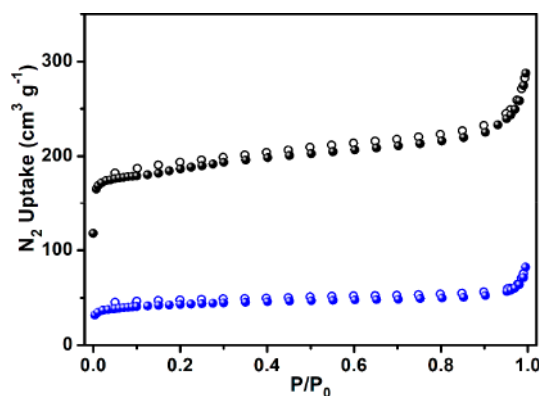
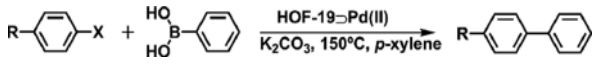


Figure 2. N_2 sorption isotherms of HOF-19a (black) and HOF-19 \supset Pd(II) (blue) at 77 K (solid symbols, adsorption; open symbols, desorption).

well with the simulated one for HOF-19 in Figure S6 (Supporting Information), indicating the hydrogen-bonded structure retained by the post-treated species and illustrating the HOF robustness again. Inductively coupled plasma (ICP) analysis gives a Pd content of 3.8 wt % included in HOF-19 \supset Pd(II). In the X-ray photoelectron spectrum shown in Figure S7 (Supporting Information), the observation of two peaks with the binding energy of 338.1 and 343.4 eV corresponding to Pd $3d_{5/2}$ and Pd $3d_{3/2}$, respectively, confirms divalent palladium ions bound by HOF-19. The slight downshift of Pd $3d_{5/2}$ and Pd $3d_{3/2}$ binding energy for HOF-19 \supset Pd(II) relative to that (338.3 and 343.6 eV) of palladium acetate indicates the presence of an interaction between Pd²⁺ ions and HOF-19.¹² The slight upshift for the binding energy of the amino group of HOF-19 after including palladium acetate not only indicates HOF-19 interacting with Pd²⁺ ions but also suggests the amino groups, instead of the intracage cavity, as active sites to bind the metal ions (Figure S8, Supporting Information). The energy-dispersive spectroscopy (EDS) mapping of HOF-19 \supset Pd(II) clearly hints at the homogeneous distribution of the Pd element, excluding the presence of Pd nanoparticles (Figure S9, Supporting Information). After postmodification with Pd(OAc)₂ to give HOF-19 \supset Pd(II) with palladium ions decorated on the surface of HOF channels, the BET surface area was decreased to $159\text{ m}^2\text{ g}^{-1}$, indicating the partial structural collapse of HOF after Pd²⁺ inclusion.

To illustrate the proof-of-concept of the HOF-based catalyst, the Suzuki–Miyaura coupling reaction was selected as a model reaction to examine the catalytic activity of HOF-19 \supset Pd(II). As can be found in Table 1, in the presence of 0.260 mmol % HOF-19 \supset Pd(II), the halogenated benzene substrates (entries 1–6) were successfully transformed to corresponding coupling products in the high isolation yields of 96–98% within a short time of 1.5–2.5 h. In particular, for the conversion of 1-bromo-4-nitrobenzene, only about 0.260% Pd content in HOF-19 \supset Pd(II) was revealed to be leached into the filtrate according to the ICP measurement, indicating the strong interaction between Pd²⁺ and HOF-19. Under the same conditions, the catalytic activity of 0.260 mmol % HOF-19 \supset Pd(II) is even comparable to the excellent performance of 0.500 mmol % COF-LZU1 \supset Pd(II) catalyst toward the reaction of 1-bromo-4-methoxybenzene with phenylboronic acid,¹² indicating the excellent catalytic activity of HOF-19 \supset Pd(II) (Table 1). Nevertheless, HOF-19 \supset Pd(II) shows a much higher catalytic efficiency in comparison with palladium acetate, a mixture of HOF-19 and

Table 1. Catalytic Performance of HOF-19Pd(II) Catalyst in the Suzuki–Miyaura Coupling Reaction^a


entry	R	X	time (h)	yield ^b (%)
1	–CHO	Br	2.5	97
2	–CN	Br	1.5	97
3	–H	Br	2.0	98
4	–NO ₂	Br	2.5	97
5	–OMe	Br	2.0	96
6	–OMe	I	1.5	97
7	–Ph	Br	4.0	19
8	–PhOMe	Br	4.0	13
9 ^c	–OMe	Br	4.0	96
10 ^d	–OMe	Br	4.0	71
11 ^e	–OMe	Br	4.0	70
12 ^f	–OMe	Br	4.0	~7
13 ^d	–Ph	Br	4.0	69
14 ^d	–PhOMe	Br	4.0	58

^aReaction conditions: aryl halide (1.00 mmol), phenylboronic acid (1.50 mmol), K₂CO₃ (2.00 mmol), HOF-19Pd(II) (7.5 mg, 0.260 mmol %), *p*-xylene (4 mL), 150 °C. ^bIsolation yield. ^c0.500 mmol % COF-LZU1Pd(II). ^d0.260 mmol % Pd(OAc)₂. ^e0.260 mmol % Pd(OAc)₂ and HOF-19 (7.5 mg). ^f0.260 mmol % Pd/C (10 wt %).

palladium acetate, and Pd/C catalyst, confirming the crucial role of palladium(II) ions deposited on the channel surfaces of HOF-19 on the present heterogeneous catalysis of the Suzuki–Miyaura coupling reaction. Interestingly, under the same reaction conditions, the substrates of 4'-bromo-1,1'-biphenyl and 4-methoxy-4'-bromo-1,1'-biphenyl with large molecular size of 7.5 × 13.9 and 7.5 × 16.0 Å, respectively, were converted into the corresponding product only with the isolation yield below 20% even after 4.0 h, which are even much lower than those with Pd(OAc)₂ as the catalyst (Table 1 and Table S3, Supporting Information), indicating the presence of pore size selectivity of the HOF-19Pd(II) catalyst.

The recyclability of HOF-19Pd(II) catalyst was evaluated in the conversion of 4-bromobenzonitrile. HOF-19Pd(II) kept an almost constant catalytic activity and good crystallinity for four cycles of reaction, indicating again the good stability of the HOF-based catalyst (Figures S6 and S10, Supporting Information). The isolated yield for the fifth reaction cycle was reduced to ca. 74%. After the continuous coupling reaction of 4-bromobenzonitrile for 20.0 h, HOF-19Pd(II) was deactivated with the low isolation yield of 46%. However, recrystallization of deactivated catalyst afforded a regenerated crystalline sample (Figure S11, Supporting Information). More importantly, this regenerated catalyst displayed a recovered catalytic activity toward 4-bromobenzonitrile with the 92% isolation yield (Figure S12, Supporting Information), revealing the sustainable advantage of this newly developed HOF-based catalyst.

In summary, a novel cage-based HOF with permanent porosity has been synthesized for the first time. Multiple hydrogen bonding interactions together with the π – π interactions enhance the stability of HOF. With this porous HOF as a robust support of palladium acetate, a highly efficient and selective HOF-based heterogeneous catalyst has been realized toward the Suzuki–Miyaura coupling reaction. In particular, by utilizing the recycling advantage of HOFs, this HOF-based catalyst could be easily regenerated through simple

recrystallization, exhibiting almost recovered activity. These results reveal the great application potentials of HOF-based catalysts. We hope the present result will ignite more research interest toward exploration of HOF-based catalysts and other applications.

■ ASSOCIATED CONTENT

Supporting Information

The Supporting Information is available free of charge on the ACS Publications website at DOI: 10.1021/jacs.9b03766.

Experimental details, NMR spectra, TGA curve, SEM photos, PXRD patterns, XPS spectra, EDS mapping of HOF-19 and/or HOF-19Pd(II) (PDF)
Crystallographic data for HOF-19 (CIF)

■ AUTHOR INFORMATION

Corresponding Authors

*hlwang@ustb.edu.cn

*banglin.chen@utsa.edu

*jianzhaung@ustb.edu.cn

ORCID

Hui Wu: 0000-0003-0296-5204

Wei Zhou: 0000-0002-5461-3617

Banglin Chen: 0000-0001-8707-8115

Jianzhuang Jiang: 0000-0002-4263-9211

Notes

The authors declare no competing financial interest.

■ ACKNOWLEDGMENTS

Financial support from the Natural Science Foundation of China (21631003 and 21805005), the Fundamental Research Funds for the Central Universities (FRF-BD-17-016A), Welch Foundation (AX-1730), National Science Foundation (DMR-1606826), and University of Science and Technology Beijing is gratefully acknowledged.

■ REFERENCES

- (1) Deutschmann, O.; Knözinger, H.; Kochloefl, K.; Turek, T. Heterogeneous Catalysis and Solid Catalysts, Fundamentals. In *Ullmann's Encyclopedia of Industrial Chemistry*; Wiley-VCH Verlag GmbH & Co. KGaA, 2000.
- (2) (a) Dusselier, M.; Davis, M. E. Small-Pore Zeolites: Synthesis and Catalysis. *Chem. Rev.* **2018**, *118*, 5265. (b) Wang, N.; Sun, Q.; Bai, R.; Li, X.; Guo, G.; Yu, J. In Situ Confinement of Ultrasmall Pd Clusters within Nanosized Silicalite-1 Zeolite for Highly Efficient Catalysis of Hydrogen Generation. *J. Am. Chem. Soc.* **2016**, *138*, 7484.
- (3) (a) Furukawa, H.; Cordova, K. E.; O'Keeffe, M.; Yaghi, O. M. The Chemistry and Applications of Metal–Organic Frameworks. *Science* **2013**, *341*, 974. (b) Xiao, J.-D.; Jiang, H.-L. Metal–Organic Frameworks for Photocatalysis and Photothermal Catalysis. *Acc. Chem. Res.* **2019**, *52*, 356. (c) Bai, Y.; Dou, Y.; Xie, L.-H.; Rutledge, W.; Li, J.-R.; Zhou, H.-C. Zr-Based Metal–Organic Frameworks: Design, Synthesis, Structure, and Applications. *Chem. Soc. Rev.* **2016**, *45*, 2327. (d) Zhu, Q.-L.; Xu, Q. Metal–Organic Framework Composites. *Chem. Soc. Rev.* **2014**, *43*, 5468. (e) Li, B.; Wen, H.-M.; Cui, Y.; Zhou, W.; Qian, G.; Chen, B. Emerging Multifunctional Metal–Organic Framework Materials. *Adv. Mater.* **2016**, *28*, 8819. (f) Drake, T.; Ji, P.; Lin, W. Site Isolation in Metal–Organic Frameworks Enables Novel Transition Metal Catalysis. *Acc. Chem. Res.* **2018**, *51*, 2129. (g) Evans, J. D.; Sumbay, C. J.; Doonan, C. J. Post-Synthetic Metalation of Metal–Organic Frameworks. *Chem. Soc. Rev.* **2014**, *43*, 5933. (h) Cohen, S. M. Postsynthetic Methods for the Functionalization of Metal–Organic Frameworks. *Chem. Rev.* **2012**, *112*, 970. (i) Bloch, E. D.; Britt, D.; Lee, C.; Doonan, C. J.; Fernando, J.

- U.-R.; Furukawa, H.; Long, J. R.; Yaghi, O. M. Metal Insertion in a Microporous Metal–Organic Framework Lined with 2,2′-Bipyridine. *J. Am. Chem. Soc.* **2010**, *132*, 14382. (j) Niu, Z.; Gunatilleke, W. D. C. B.; Sun, Q.; Lan, P. C.; Perman, J.; Ma, J.-G.; Cheng, Y.; Aguila, B.; Ma, S. Metal–Organic Framework Anchored with a Lewis Pair as a New Paradigm for Catalysis. *Chem.* **2018**, *4*, 2587. (k) Liu, J.; Ye, J.; Li, Z.; Otake, K.-I.; Liao, Y.; Peters, A. W.; Noh, H.; Truhlar, D. G.; Gagliardi, L.; Cramer, C. J.; Farha, O. K.; Hupp, J. T. Beyond the Active Site: Tuning the Activity and Selectivity of a Metal–Organic Framework-Supported Ni Catalyst for Ethylene Dimerization. *J. Am. Chem. Soc.* **2018**, *140*, 11174. (l) Liao, P.-Q.; Shen, J.-Q.; Zhan, J.-P. Metal–Organic Frameworks for Electrocatalysis. *Coord. Chem. Rev.* **2018**, *373*, 22. (m) He, W.-L.; Zhao, M.; Wu, C.-D. A Versatile Metalloporphyrinic Framework Platform for Highly Efficient Bioinspired, Photo- and Asymmetric Catalysis. *Angew. Chem., Int. Ed.* **2019**, *58*, 168.
- (4) (a) Lin, S.; Diercks, C. S.; Zhang, Y.-B.; Kornienko, N.; Nichols, E. M.; Zhao, Y.; Paris, A. R.; Kim, D.; Yang, P.; Yaghi, O. M.; Chang, C. J. Covalent Organic Frameworks Comprising Cobalt Porphyrins for Catalytic CO₂ Reduction in Water COF. *Science* **2015**, *349*, 1208. (b) Lu, S.; Hu, Y.; Wan, S.; McCaffrey, R.; Jin, Y.; Gu, H.; Zhang, W. Synthesis of Ultrafine and Highly Dispersed Metal Nanoparticles Confined in a Thioether-Containing Covalent Organic Framework and Their Catalytic Applications. *J. Am. Chem. Soc.* **2017**, *139*, 17082.
- (5) (a) Barrer, R. M.; Shanson, V. H. Dianin's Compound as a Zeolitic Sorbent. *J. Chem. Soc., Chem. Commun.* **1976**, *9*, 333. (b) Lee, F.; Gabe, E.; Tse, J. S.; Ripmeester, J. A. Crystal Structure, CP/MAS ¹²⁹Xe, and ¹³C NMR of Local Ordering in Dianin's Compound Clathrates. *J. Am. Chem. Soc.* **1988**, *110*, 6014. (c) Lloyd, G. O.; Bredenkamp, M. W.; Barbour, L. J. Enclathration of Morpholinium Cations by Dianin's Compound: Salt Formation by Partial Host-to-Guest Proton Transfer. *Chem. Commun.* **2005**, 4053. (d) Simard, M.; Su, D.; Wuest, J. D. Use of Hydrogen Bonds to Control Molecular Aggregation. Self-Assembly of Three-Dimensional Networks with Large Chambers. *J. Am. Chem. Soc.* **1991**, *113*, 4696. (e) McKeown, N. B. Nanoporous Molecular Crystals. *J. Mater. Chem.* **2010**, *20*, 10588. (f) Adachi, T.; Ward, M. D. Versatile and Resilient Hydrogen-Bonded Host Frameworks. *Acc. Chem. Res.* **2016**, *49*, 2669. (g) Lin, R.; He, Y.; Li, P.; Wang, H.; Zhou, W.; Chen, B. Multifunctional Porous Hydrogen-Bonded Organic Framework Materials. *Chem. Soc. Rev.* **2019**, *48*, 1362. (h) Brunet, P.; Simard, M.; Wuest, J. D. Molecular Tectonics. Porous Hydrogen-Bonded Networks with Unprecedented Structural Integrity. *J. Am. Chem. Soc.* **1997**, *119*, 2737. (i) Luo, J.; Wang, J.-W.; Zhang, J.-H.; Lai, S.; Zhong, D.-C. Hydrogen-Bonded Organic Frameworks: Design, Structures and Potential Applications. *CrystEngComm* **2018**, *20*, 5884. (j) Endo, K.; Sawaki, T.; Koyanagi, M.; Kobayashi, K.; Masuda, H.; Aoyama, Y. Guest-Binding Properties of Organic Crystals Having an Extensive Hydrogen-Bonded Network: An Orthogonal Anthracene-Bis-(resorcinol) Derivative as a Functional Organic Analog of Zeolites. *J. Am. Chem. Soc.* **1995**, *117*, 8341. (k) Saied, O.; Maris, T.; Wuest, J. D. Deformation of Porous Molecular Networks Induced by the Exchange of Guests in Single Crystals. *J. Am. Chem. Soc.* **2003**, *125*, 14956. (l) Kobayashi, K.; Sato, A.; Sakamoto, S.; Yamaguchi, K. Solvent-Induced Polymorphism of Three-Dimensional Hydrogen-Bonded Networks of Hexakis(4-carbamoylphenyl)benzene. *J. Am. Chem. Soc.* **2003**, *125*, 3035. (m) Liu, Y.; Hu, C.; Comotti, A.; Ward, M. D. Supramolecular Archimedean Cages Assembled with 72 Hydrogen Bonds. *Science* **2011**, *333*, 436. (n) Soldatov, D. V.; Moudrakovski, I. L.; Grachev, E. V.; Ripmeester, J. A. Micropores in Crystalline Dipeptides as Seen from the Crystal Structure, He Pycnometry, and ¹²⁹Xe NMR Spectroscopy. *J. Am. Chem. Soc.* **2006**, *128*, 6737. (o) Tian, J.; Thallapally, P. K.; Dalgarno, S. J.; Atwood, J. L. Free Transport of Water and CO₂ in Nonporous Hydrophobic Clarithromycin Form II Crystals. *J. Am. Chem. Soc.* **2009**, *131*, 13216.
- (6) (a) Dalrymple, S. A.; Shimizu, G. K. H. Crystal Engineering of a Permanently Porous Network Sustained Exclusively by Charge-Assisted Hydrogen Bonds. *J. Am. Chem. Soc.* **2007**, *129*, 12114. (b) Hisaki, I.; Nakagawa, S.; Tohnai, N.; Miyata, M. A C₃-Symmetric Macrocyclic-Based, Hydrogen-Bonded, Multiporous Hexagonal Network as a Motif of Porous Molecular Crystals. *Angew. Chem., Int. Ed.* **2015**, *54*, 3008. (c) Hu, F.; Liu, C.; Wu, M.; Pang, J.; Jiang, F.; Yuan, D.; Hong, M. An Ultrastable and Easily Regenerated Hydrogen-Bonded Organic Molecular Framework with Permanent Porosity. *Angew. Chem., Int. Ed.* **2017**, *56*, 2101. (d) Mastalerz, M.; Oppel, I. M. Rational Construction of an Extrinsic Porous Molecular Crystal with an Extraordinary High Specific Surface Area. *Angew. Chem., Int. Ed.* **2012**, *51*, 5252. (e) Pulido, A.; Chen, L.; Kaczorowski, T.; Holden, D.; Little, M. A.; Chong, S. Y.; Slater, B. J.; McMahon, D. P.; Bonillo, B.; Stackhouse, C. J.; Stephenson, A.; Kane, C. M.; Clowes, R.; Hasell, T.; Cooper, A. I.; Day, G. M. Functional Materials Discovery Using Energy-Structure-Function Maps. *Nature* **2017**, *543*, 657. (f) Yin, Q.; Zhao, P.; Sa, R.-J.; Chen, G.-C.; Lü, J.; Liu, T.-F.; Cao, R. An Ultra-Robust and Crystalline Redeemable Hydrogen-Bonded Organic Framework for Synergistic Chemo-Photodynamic Therapy. *Angew. Chem., Int. Ed.* **2018**, *57*, 7691.
- (7) (a) Chen, T.-H.; Popov, I.; Kaveevivitchai, W.; Chuang, Y.-C.; Chen, Y.; Daugulis, O.; Jacobson, A. J.; Miljanić, O. Š. Thermally Robust and Porous Noncovalent Organic Framework with High Affinity for Fluorocarbons and CFCs. *Nat. Commun.* **2014**, *5*, 5131. (b) Luo, X.-Z.; Jia, X.-J.; Deng, J.-H.; Zhong, J.-L.; Liu, H.-J.; Wang, K.-J.; Zhong, D.-C. A Microporous Hydrogen-Bonded Organic Framework: Exceptional Stability and Highly Selective Adsorption of Gas and Liquid. *J. Am. Chem. Soc.* **2013**, *135*, 11684. (c) He, Y.; Xiang, S.; Chen, B. A Microporous Hydrogen-Bonded Organic Framework for Highly Selective C₂H₂/C₂H₄ Separation at Ambient Temperature. *J. Am. Chem. Soc.* **2011**, *133*, 14570. (d) Li, P.; He, Y.; Zhao, Y.; Weng, L.; Wang, H.; Krishna, R.; Wu, H.; Zhou, W.; O'Keeffe, M.; Han, Y.; Chen, B. A Rod-Packing Microporous Hydrogen-Bonded Organic Framework for Highly Selective Separation of C₂H₂/CO₂ at Room Temperature. *Angew. Chem., Int. Ed.* **2014**, *54* (2), 574–577. (e) Li, P.; He, Y.; Guang, J.; Weng, L.; Zhao, J. C.-G.; Xiang, S.; Chen, B. A Homochiral Microporous Hydrogen-Bonded Organic Framework for Highly Enantio Selective Separation of Secondary Alcohols. *J. Am. Chem. Soc.* **2014**, *136*, 547. (f) Wang, H.; Li, B.; Wu, H.; Hu, T.-L.; Yao, Z.; Zhou, W.; Xiang, S.; Chen, B. A Flexible Microporous Hydrogen-Bonded Organic Framework for Gas Sorption and Separation. *J. Am. Chem. Soc.* **2015**, *137*, 9963. (g) Bao, Z.; Xie, D.; Chang, G.; Wu, H.; Li, L.; Zhou, W.; Wang, H.; Zhang, Z.; Xing, H.; Yang, Q.; Zaworotko, M. J.; Ren, Q.; Chen, B. Fine Tuning and Specific Binding Sites with a Porous Hydrogen-Bonded Metal-Complex Framework for Gas Selective Separations. *J. Am. Chem. Soc.* **2018**, *140*, 4596. (h) Zhou, D.-D.; Xu, Y.-T.; Lin, R.-B.; Mo, Z.-W.; Zhang, W.-X.; Zhang, J.-P. High-Symmetry Hydrogen-Bonded Organic Frameworks: Air Separation and Crystal-to-Crystal Structural Transformation. *Chem. Commun.* **2016**, *52*, 4991.
- (8) Hisaki, I.; Suzuki, Y.; Gomez, E.; Ji, Q.; Tohnai, N.; Nakamura, T.; Douhal, A. Acid Responsive Hydrogen-Bonded Organic Frameworks. *J. Am. Chem. Soc.* **2019**, *141*, 2111.
- (9) (a) Xing, G.; Yan, T.; Das, S.; Ben, T.; Qiu, S. Synthesis of Crystalline Porous Organic Salts with High Proton Conductivity. *Angew. Chem., Int. Ed.* **2018**, *57*, 5345. (b) Karmakar, A.; Illathalappil, R.; Anothumakkool, B.; Sen, A.; Samanta, P.; Desai, A. V.; Kurungot, S.; Ghosh, S. K. Hydrogen-Bonded Organic Frameworks (HOFs): A New Class of Porous Crystalline Proton-Conducting Materials. *Angew. Chem., Int. Ed.* **2016**, *55*, 10667.
- (10) Wang, D.-X.; Wang, Q.-Q.; Han, Y.; Wang, Y.; Huang, Z.-T.; Wang, M.-X. Versatile Anion-Interactions between Halides and a Conformationally Rigid Bis(tetraoxacalix[2]arene[2]triazine) Cage and Their Directing Effect on Molecular Assembly. *Chem. - Eur. J.* **2010**, *16*, 13053.
- (11) Spek, A. L. *PLATON: A Multipurpose Crystallographic Tool*; Utrecht University, Utrecht, The Netherlands, 2005.
- (12) Ding, S.-Y.; Gao, J.; Wang, Q.; Zhang, Y.; Song, W.-G.; Su, C.-Y.; Wang, W. Construction of Covalent Organic Framework for Catalysis: Pd/COF-LZU1 in Suzuki-Miyaura Coupling Reaction. *J. Am. Chem. Soc.* **2011**, *133*, 19816.

Supporting Information

Post-Synthetic Metalation of Robust Hydrogen-Bonded Organic Framework for Heterogeneous Catalysis

Bin Han,[†] Hailong Wang,^{*,†} Chiming Wang,[†] Hui Wu,[§] Wei Zhou,[§] Banglin Chen,^{*,‡}

Jianzhuang Jiang^{*,†}

[†] Beijing Key Laboratory for Science and Application of Functional Molecular and Crystalline Materials,
Department of Chemistry, University of Science and Technology Beijing, Beijing 100083, China

[‡] Department of Chemistry, University of Texas at San Antonio, San Antonio, Texas 78249-0698, United
States

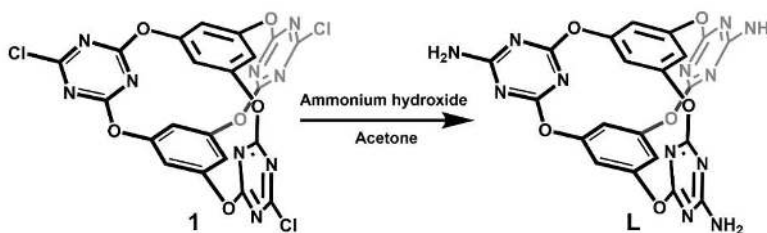
[§] Center for Neutron Research, National Institute of Standards and Technology, Gaithersburg,
Maryland 20899-6102, United States

Caption of Content

Experimental section	S3
Figure S1. ^1H NMR spectrum of L in $\text{DMSO}-d_6$	S10
Figure S2. ^{13}C NMR spectrum of L in $\text{DMSO}-d_6$	S10
Figure S3. TGA curve of as-synthesized HOF-19.....	S11
Figure S4. PXRD patterns of HOF-19 and HOF-19a.....	S11
Figure S5. SEM photos of HOF-19a and HOF-19 \supset Pd(II)	S12
Figure S6. PXRD pattern of HOF-19 \supset Pd(II) after four cycles of reaction.....	S12
Figure S7. XPS Pd 3d spectra of HOF-19 \supset Pd(II) and $\text{Pd}(\text{OAc})_2$	S13
Figure S8. XPS N 1s spectra of HOF-19 and HOF-19 \supset Pd(II).....	S13
Figure S9. EDS mapping of HOF-19 \supset Pd(II).....	S14
Figure S10. Recycle test of HOF-19 \supset Pd(II).....	S14
Figure S11. PXRD pattern of regenerated catalyst.....	S15
Figure S12. Catalytic performance of regenerated HOF-19 \supset Pd(II).....	S15
Table S1. Crystallographic and refinement parameters for HOF-19.....	S16
Table S2. Hydrogen bonding interaction in the crystal structure of HOF-19.....	S17
Table S3. Molecular sizes of 4-bromo-1,1'-biphenyl and 4-bromo-4'-methoxy-1,1'-biphenyl.....	S17
Reference	S18

Experimental Section.

General information. All chemicals were obtained from commercial sources and used without further purification. **1** was prepared according to the published procedure.^[S1]



Scheme S1. Schematic synthesis of the building block (**L**) for the assembly of HOF-19.

Synthesis of L and HOF-19. To a solution of **1** (585 mg, 1.00 mmol) in acetone (30 mL), ammonium hydroxide (250 μL , 28%) was added, Scheme S1. The resulting mixture was stirred over night at room temperature. The white solid was obtained by filtration and washing with acetone (10 mL \times 3) and water (10 mL \times 3). The product **L** was dried at room temperature and obtained with the yield of 72% (370 mg). ^1H NMR (DMSO- d_6 , 400 MHz): δ (ppm) 7.77 (s, 6H), 6.70 (s, 6H). ^{13}C NMR (DMSO- d_6 , 100 MHz): δ (ppm) 172.02, 170.02, 152.72, 114.96. Anal. Calcd for $\text{C}_{21}\text{H}_{12}\text{N}_{12}\text{O}_6 \cdot \text{H}_2\text{O}$: C 46.16; H 2.58; N 30.76. Found: C 46.11; H 2.51; N 30.81. The single crystals of HOF-19 were obtained by the slow evaporation of formic acid solution containing **L**, and bulk material of this HOF was prepared by the slow diffusion of acetone into formic acid solution in a yield of 50%.

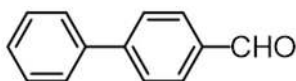
Synthesis of HOF-19 \Rightarrow Pd(II) and regeneration of HOF-based catalyst. HOF-19a (53.0 mg) was immersed in an acetone solution (10 mL) containing palladium acetate (22.4 mg, 0.100 mmol) for 12.0 hours at room temperature. The resulting solid was isolated by centrifugation and washed with acetone and water for three times, and dried under vacuum at room temperature for 6.0 hours to yield HOF-19 \Rightarrow Pd(II) (68.0 mg) as a brown powder. The Pd content in HOF-19 \Rightarrow Pd(II) is 3.8 wt% as determined by ICP.

The deactivated catalyst was obtained after the continuous coupling reaction of phenylboronic acid (1.83 g \times 5) and 4-bromobenzonitrile (2.02 g \times 5) in the presence of K₂CO₃ (2.76 g) with the help of HOF-19 \Rightarrow Pd(II) (150 mg) in *p*-xylene (40 mL) for 20.0 hours. The catalyst was separated by centrifugation and washed by *p*-xylene (20 mL \times 3), water (20 mL \times 3), and acetone (20 mL \times 3), which was dried at room temperature and obtained in a yield of *ca.* 89% (134 mg). The regenerated HOF-based catalyst was obtained by the same synthesis method of HOF-19 bulk material, by diffusing acetone into a formic acid solution (10 mL) of the deactivated species (134 mg). After five days, the regenerated species was collected by filtration and dried at room temperature, which was obtained in a yield of 41% (55.1 mg).

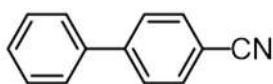
Catalytic activity test of HOF-19 \Rightarrow Pd(II). In a typical run of catalytic activity test, aryl halide (1.00 mmol), phenylboronic acid (183 mg, 1.50 mmol), K₂CO₃ (276 mg, 2.00 mmol), and HOF-19 \Rightarrow Pd(II) (7.5 mg, 0.260 mmol%) were added to *p*-xylene (4 mL), which were stirred at 150°C at N₂ atmosphere and monitored by thin-layer

chromatography (TLC). After the reaction completed, the mixture was centrifuged, and the organic phase was separated. The solid was washed with dichloromethane (3 × 5 mL). The organic phases were combined and washed with water (20 mL) to remove K₂CO₃ residue. The combined organic phase was then evaporated under vacuum to give the crude product. The crude product was further purified by column chromatography over silica gel to obtain the target product.

In the recycle test, the reaction of 4-bromobenzonitrile (182 mg, 1.00 mmol) with phenylboronic acid (183 mg, 1.50 mmol) in presence of K₂CO₃ (276 mg, 2.00 mmol), HOF-19-Pd(II) (15.0 mg, 0.520 mmol%), and *p*-xylene (4 mL) was carried out. After each cycle, the catalyst was separated by centrifugation and washed by *p*-xylene (3 mL × 3), which was used directly in the next cycle of reaction.

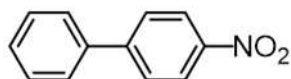


Prepared according to the aforementioned procedure with 4-bromobenzaldehyde as starting material. The product was collected as a white solid with a yield of 97% (177 mg) after silica gel chromatography (dichloromethane:*n*-hexane = 1:2). ¹H NMR (400 MHz, CDCl₃): δ (ppm) 10.01 (s, 1H), 7.97 (d, *J* = 8.0 Hz, 2H), 7.77 (d, *J* = 8.0 Hz 2H), 7.66 (d, *J* = 8.0 Hz, 2H), 7.51-7.47 (m, 2H), 7.44-7.40 (m, 1H).

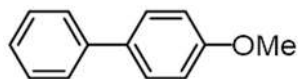


Prepared according to the aforementioned procedure with 4-bromobenzonitrile as

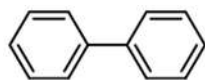
starting material. The product was collected as white solid with a yield of 97% (174 mg) after silica gel chromatography (dichloromethane:petroleum ether = 2:3). ^1H NMR (400 MHz, CDCl_3): δ (ppm) 7.74-7.68 (m, 4H), 7.60 (d, $J = 8.0$ Hz, 2H), 7.51 (m, 3H).



Prepared according to the aforementioned procedure with 1-bromo-4-nitrobenzene as starting material. The product was collected as a pale yellow solid with a yield of 97% (193 mg) after silica gel chromatography (dichloromethane:*n*-hexane = 1:2). ^1H NMR (400 MHz, CDCl_3): δ (ppm) 8.32 (d, $J = 8.0$ Hz, 2H), 7.76 (d, $J = 8.0$ Hz, 2H), 7.64 (d, $J = 8.0$ Hz, 2H), 7.52-7.43 (m, 3H).

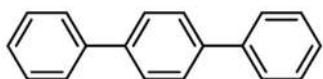


Prepared according to the aforementioned procedure with 4-bromoanisole (or 4-iodoanisole) as starting material. The product was collected as a white solid with a yield of 96% (177 mg) from 4-bromoanisole as starting material and 97% (179 mg) from 4-iodoanisole as starting material after silica gel chromatography (dichloromethane:*n*-hexane = 1:3). ^1H NMR (400 MHz, CDCl_3): δ (ppm) 7.56-7.52 (m, 4H), 7.44 (t, $J = 8.0$ Hz, 2H), 7.32-7.29 (m, 1H), 6.99 (d, $J = 8.0$ Hz, 2H), 3.86 (s, 3H).

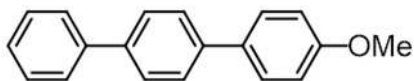


Prepared according to the aforementioned procedure with 4-bromobenzene as

starting material. The product was collected as colorless oil with a yield of 98% (151 mg) after silica gel chromatography (petroleum ether). ^1H NMR (400 MHz, CDCl_3): δ (ppm) 7.61 (d, $J = 8.0$ Hz, 4H), 7.46 (t, $J = 8.0$ Hz, 4H), 7.37 (t, $J = 8.0$ Hz, 2H).



Prepared according to the aforementioned procedure with 4-bromobiphenyl as starting material. The product was collected as a white solid with a yield of 19% (43.7 mg) after silica gel chromatography (dichloromethane:*n*-hexane = 1:9). ^1H NMR (400 MHz, CDCl_3): δ (ppm) 7.69 (s, 4H), 7.66-7.64 (m, 4H), 7.49 (t, $J = 7.6$ Hz, 4H), 7.39 (t, $J = 7.6$ Hz, 2H).



Prepared according to the aforementioned procedure with 4-bromo-4'-methoxybiphenyl as starting material. The product was collected as a white solid with a yield of 13% (33.8 mg) after silica gel chromatography (dichloromethane:*n*-hexane = 1:4). ^1H NMR (400 MHz, CDCl_3): δ (ppm) 7.67-7.58 (m, 8H), 7.51-7.44 (m, 2H), 7.40 (t, $J = 7.6$ Hz, 1H), 7.00 (d, $J = 8.8$ Hz, 2H), 3.87 (s, 3H).

Physical characterization. NMR spectra were recorded on a Bruker DPX 400 spectrometer (^1H : 400 MHz, ^{13}C : 100 MHz) in CDCl_3 and $\text{DMSO}-d_6$. ^1H NMR spectra were referenced internally using the residual solvent resonances ($\delta = 7.26$ ppm for

CDCl₃ and $\delta = 2.50$ ppm for DMSO-*d*₆) relative to SiMe₄. ¹³C NMR spectrum was referenced internally by using the solvent resonance ($\delta = 39.52$ ppm for DMSO-*d*₆). Elemental analysis was performed on an Elementar Vavio El III. Powder X-ray diffraction (PXRD) data were collected with a TTR III multi-function X-ray diffractometer operated at 40 kV and 300 mA with Cu K α radiation. X-ray photoelectron spectroscopy (XPS) data were conducted on an ESCALAB 250Xi system. Al K α X-ray (6 mA \times 12 KV) was utilized as the irradiation source. All measurements were performed in the CAE mode with the reference of C 1s (284.8 eV). The nitrogen adsorption and desorption isotherms were measured at 77 K using a Micromeritics ASAP 2020 PLUS HD88 system. The samples were degassed at room temperature for 24.0 hours before the measurement. The thermogravimetric analysis (TGA) was performed on a Perkin-Elmer instrument over the temperature range of 25 to 800°C under nitrogen atmosphere with a heating rate of 10°C/min. The Pd content of the HOF-19 \Rightarrow Pd(II) sample was determined by inductively coupled plasma (ICP) analysis with an Agilent 7700X ICP-MS instrument. Energy dispersive spectroscopy (EDS) mapping images were collected by transmission electron microscopy (JEM-2100F) at an operation voltage of 200 kV. Scanning electron microscopy (SEM) images were performed on a HITACHI SU8010 microscope operated at an accelerating voltage of 3.0 KV.

Single crystal crystallography. Crystallographical data of HOF-19 was collected on a diffractometer of SuperNova, Dual, Cu at home/near, AtlasS2 with Cu K α radiation

($\lambda = 1.54184 \text{ \AA}$) at 200.00 K. The structure was solved by the direct method (SHELXS-2014) and refined by full-matrix least-squares (SHELXL-2014) on F^2 .^[S2] Anisotropic thermal parameters were used for the non-hydrogen atoms and isotropic parameters for the hydrogen atoms. Hydrogen atoms were added geometrically and refined using a riding model. Because there are seriously disordered solvent molecules in the HOF-19 pores, 'SQUEEZE' command was employed. CCDC 1900772 for HOF-19 contains the supplementary crystallographic data for this paper. These data can be obtained free of charge from the Cambridge Crystallographic Data Centre via www.ccdc.cam.ac.uk/data_request/cif.

Theoretical simulation. For the purpose of theoretically determining the molecular sizes of selected reaction substrates, density functional theory (DFT) calculations were carried out on the basis of B97XD/BS1^[S3] using Gaussian 09 D.01 software package.^[S4] The BSI represents a mix basis sets where 6-311G(d)^[S5] for C, H, O, and N atoms and LanL2DZ^[S6] for Br atom.

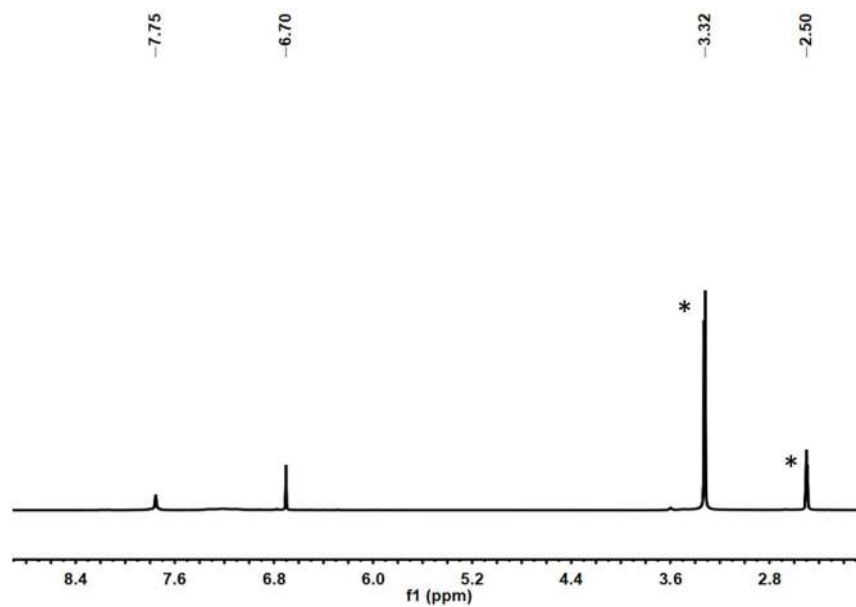


Figure S1. ^1H NMR spectrum of **L** in $\text{DMSO-}d_6$. * denotes the solvent impurity in $\text{DMSO-}d_6$.

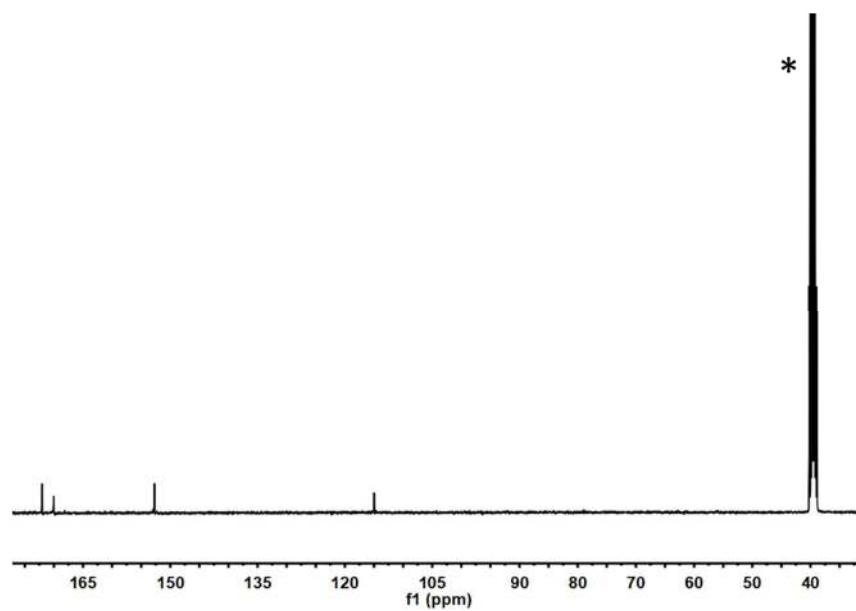


Figure S2. ^{13}C NMR spectrum of **L** in $\text{DMSO-}d_6$. * denotes the solvent impurity in $\text{DMSO-}d_6$.

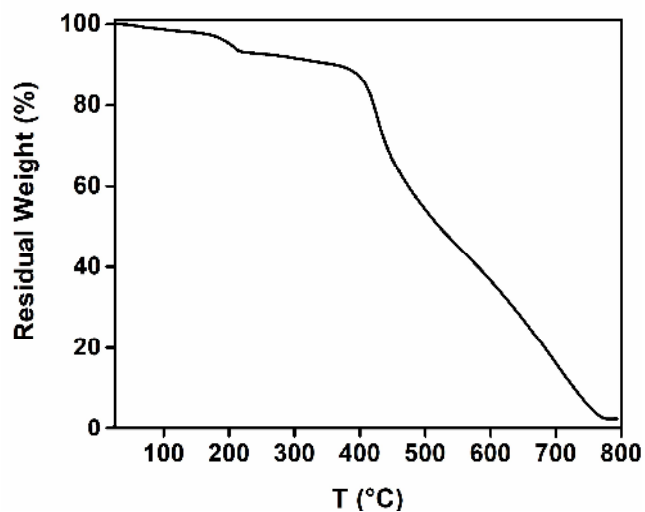


Figure S3. TGA curve of as-synthesized HOF-19 in the range of 25 to 800°C.

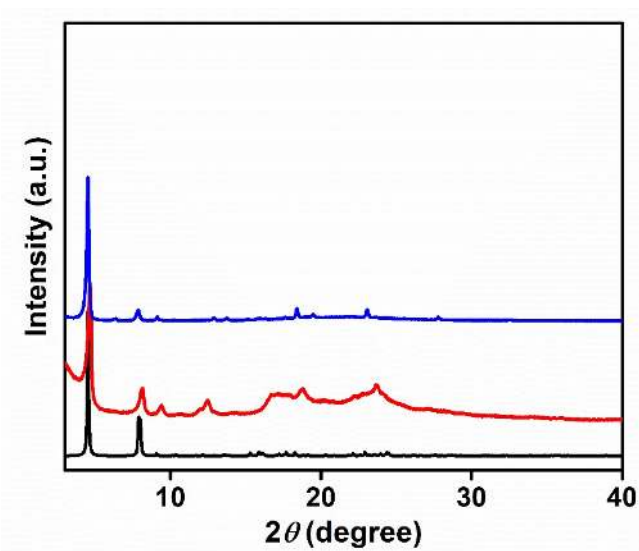


Figure S4. PXRD profiles of as-synthesized HOF-19 (red) and HOF-19a (blue) in comparison with a simulated powder pattern based on the single-crystal structure of HOF-19 without the solvent molecules included (black).

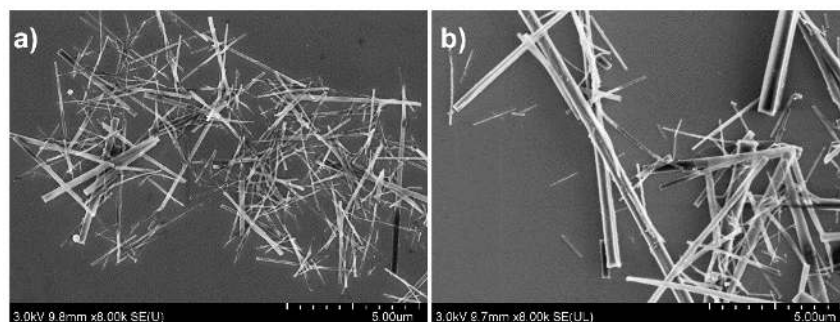


Figure S5. SEM photos of (a) activated HOF-19a and (b) HOF-19 \supset Pd(II).

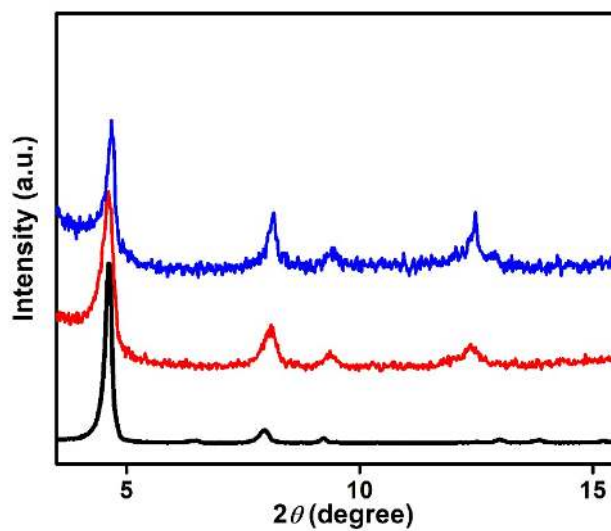


Figure S6. PXRD profiles of HOF-19a (black), HOF-19 \supset Pd(II) (red), and HOF-19 \supset Pd(II) after four cycles of reaction (blue).

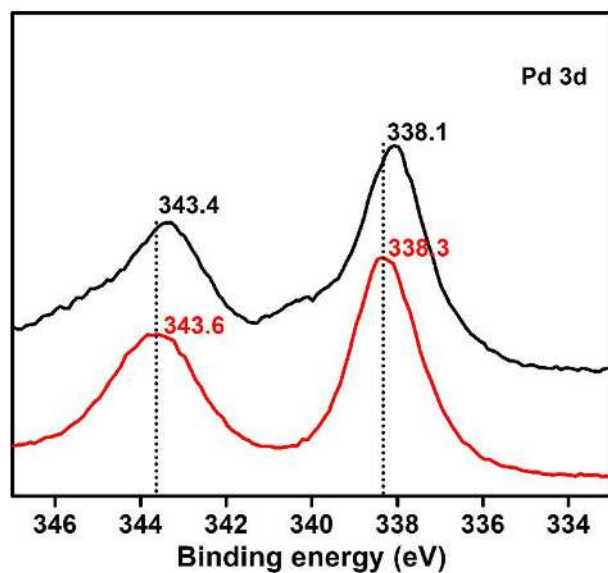


Figure S7. XPS spectra of HOF-19-Pd(II) (black) and Pd(OAc)₂ (red).

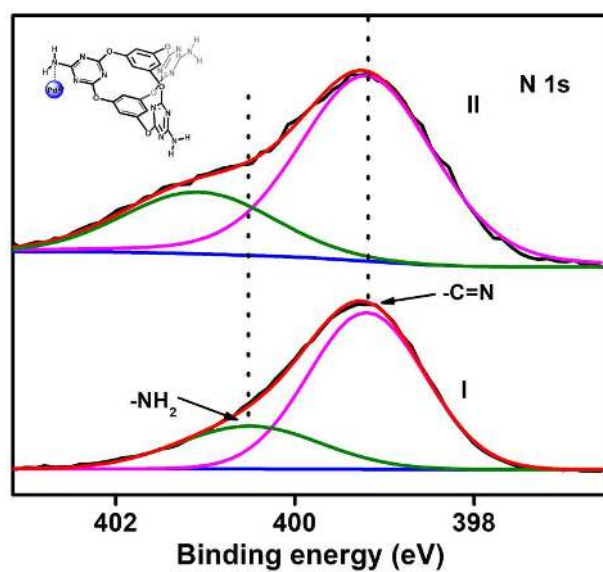


Figure S8. XPS deconvolution of HOF-19 (I) and HOF-19-Pd(II) (II) and possible amino binding site to complex with palladium ion (insert). Experimental spectra (black); background spectra (blue); Voigt curves (green and pink); simulated spectra comprising the sum of the Voigt curves (red).

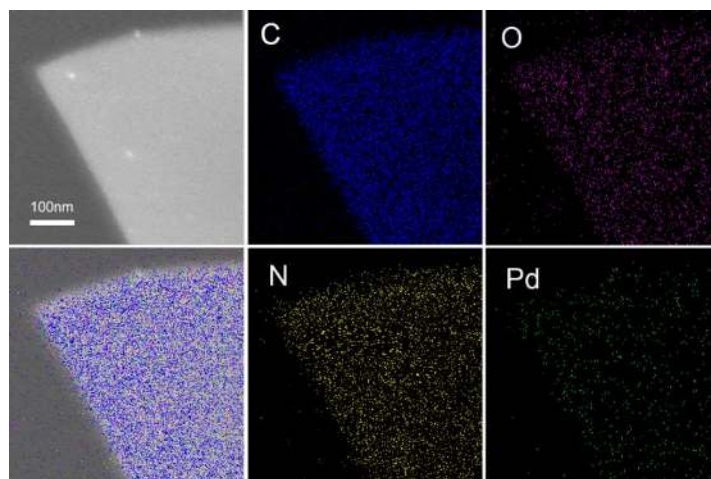


Figure S9. EDS mapping of HOF-19-Pd(II).

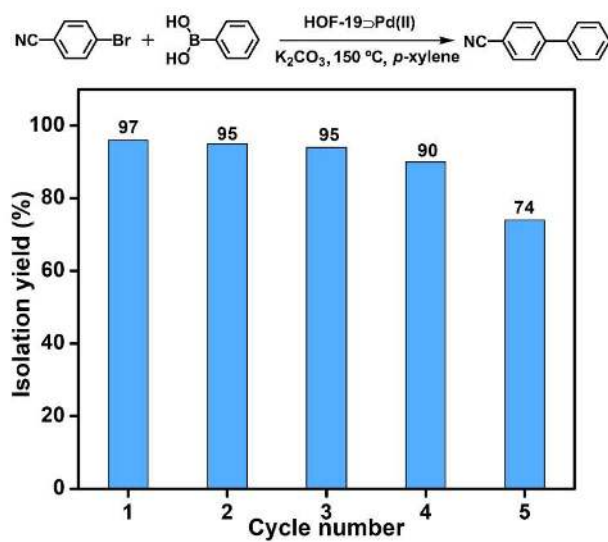


Figure S10. Recycle test of HOF-19-Pd(II) in the Suzuki-Miyaura coupling reaction of 4-bromobenzonitrile and phenylboronic acid (The reaction conditions: 4-bromobenzonitrile (1.00 mmol), phenylboronic acid (1.50 mmol), K_2CO_3 (2.00 mmol), and HOF-19-Pd(II) (15.0 mg), *p*-xylene (4 mL), 150°C, 2.0 hours).

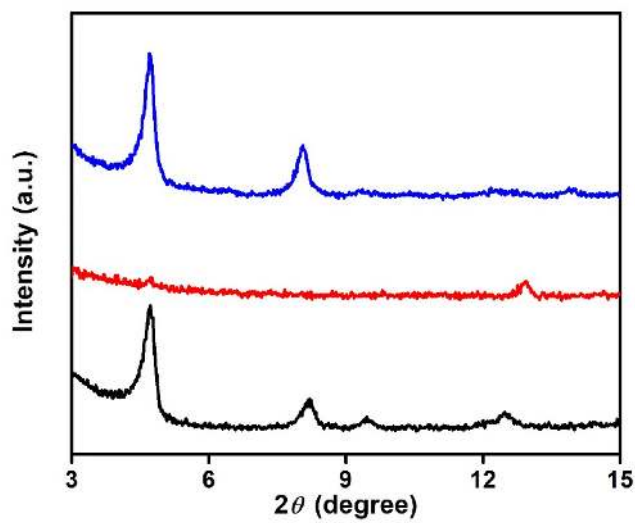


Figure S11. PXRD profiles of regenerated HOF-19Pd(II) (blue) and deactivated HOF-19Pd(II) (red) in comparison with that of as synthesized HOF-19Pd(II) (black).

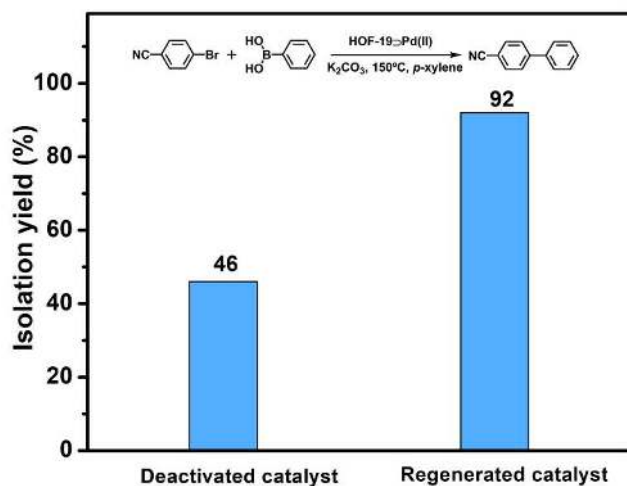


Figure S12. Catalytic performance of deactivated HOF-19Pd(II) (7.5 mg) and regenerated species (7.5 mg) in the Suzuki-Miyaura coupling reaction of 4-bromobenzonitrile (1.00 mmol) with phenylboronic acid (1.50 mmol) in the presence of K₂CO₃ (2.00 mmol) in p-xylene (4 mL) at 150°C in 3.0 hours.

Table S1. Crystallographic and refinement parameters for HOF-19.

crystal data	HOF-19
system	monoclinic
space group	<i>C2/m</i>
MF	C ₂₁ H ₁₂ N ₁₂ O ₆
FW	528.43
<i>a</i> /Å	23.0932(15)
<i>b</i> /Å	8.0164(4)
<i>c</i> /Å	20.0514(18)
α /°	90
β /°	105.212(8)
γ /°	90
volume /Å ³	3581.9(5)
Z	4
density /g/cm ³	0.98
solvent-accessible void space /% ^[S7]	47
theoretical pore volume /cm ³ /g	0.48
refinement parameters	$R_1 = 0.0740^{[a]}$, $wR_2 = 0.2254^{[b]}$

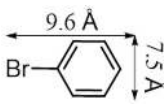
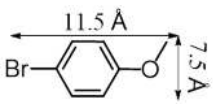
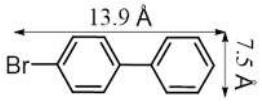
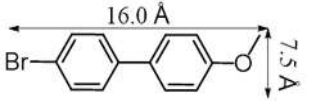
^[a] $R_1 = \Sigma |F_o| - |F_c| / \Sigma |F_o|$; ^[b] $wR_2 = [\Sigma w(F_o^2 - F_c^2)^2 / \Sigma w(F_o^2)^2]^{1/2}$.

Table S2. Hydrogen bonding interaction in the crystal structure of HOF-19.

D-H...A	distance(H...A) / Å	distance (D...A) / Å	angle(DHA) / °
N(1)-H(1B)...N(8)#2	2.25	3.060(3)	158.2
N(1)-H(1A)...N(8)#3	2.24	3.060(3)	158.7
N(2)-H(2B)...N(6)#4	2.21	3.065(3)	170.4
N(2)-H(2A)...N(6)#5	2.21	3.065(3)	170.4
N(3)-H(3B)...N(4)#6	2.25	3.061(3)	158.2
N(3)-H(3A)...N(4)#7	2.25	3.061(3)	158.5
N(1)-H(1B)...N(8)#2	2.25	3.060(3)	158.2
N(1)-H(1A)...N(8)#3	2.24	3.060(3)	158.7
N(2)-H(2B)...N(6)#4	2.21	3.065(3)	170.4
N(2)-H(2A)...N(6)#5	2.21	3.065(3)	170.4
N(3)-H(3B)...N(4)#6	2.25	3.061(3)	158.2
N(3)-H(3A)...N(4)#7	2.25	3.061(3)	158.5

^[a] Symmetric code for HOF-19: #1 x, -y+1, z; #2 x-1/2, y+1/2, z; #3 x-1/2, -y+1/2, z; #4 -x+1/2, y+1/2, -z+1; #5 -x+1/2, -y+1/2, -z+1; #6 x+1/2, -y+1/2, z; #7 x+1/2, y+1/2, z.

Table S3. Comparison of molecular sizes of bromobenzene (entry 1), 1-bromo-4-methoxybenzene (entry 2), 4-bromo-1,1'-biphenyl (entry 3), and 4-bromo-4'-methoxy-1,1'-biphenyl (entry 4).

Entry	Molecular size	Entry	Molecular size
1		2	
3		4	

Reference:

- (S1) Wang, D.-X.; Wang, Q.-Q.; Han, Y.; Wang, Y.; Huang, Z.-T.; Wang, M.-X. Versatile Anion- π Interactions between Halides and a Conformationally Rigid Bis(tetraoxacalix[2]arene[2]triazine) Cage and Their Directing Effect on Molecular Assembly. *Chem. Eur. J.* **2010**, *16*, 13053.
- (S2) Sheldrick, G. M. *SHELXL-2014*; University of Göttingen, Göttingen, Germany, **2014**.
- (S3) Chai, J.-D.; Martin, H.-G. Long-Range Corrected Hybrid Density Functionals with Damped Atom-Atom Dispersion Corrections. *Phys. Chem. Chem. Phys.* **2008**, *10*, 6615.
- (S4) Frisch, M. J., et al., Gaussian 09, Revision D.01; Gaussian, Inc.: Wallingford CT, **2010**.
- (S5) (a) McLean, A. D.; Chandler, G. S. Contracted Gaussian Basis Sets for Molecular Calculations. I. Second Row Atoms, Z=11-18. *J. Chem. Phys.* **1980**, *72*, 5639. (b) Krishnan, R.; Binkley, J. S.; Seeger, R.; Pople, J. A. Self-Consistent Molecular Orbital Methods. XX. A Basis Set for Correlated Wave Functions. *J. Chem. Phys.* **1980**, *72*, 650.
- (S6) Hay, P. J.; Wadt, W. R. Ab Initio Effective Core Potentials for Molecular Calculations. Potentials for the Transition Metal Atoms Sc to Hg. *J. Chem. Phys.* **1985**, *82*, 270.
- (S7) Spek, A. L. PLATON, A Multipurpose Crystallographic Tool; Utrecht University: Utrecht, the Netherlands, **2005**.